Proceedings World Geothermal Congress 2020+1
Reykjavik, Iceland, April - October 2021

Phase Behavior of Nitrogen Transport in Fractures During Liquid Nitrogen Fracturing in Deep Geothermal Reservoirs

Haitao Wen[1], Ruiyue Yang[1]*, Zhongwei Huang[1], Chunyang Hong[1], Jianxiang Chen[1], Guofeng Song[1]

[1]State Key Laboratory of Petroleum Resources and Prospecting, China University of Petroleum, Beijing, Beijing 102249, China

yangruiyue@cup.edu.cn

Keywords: Geothermal Reservoir, Unsteady-state Model, Liquid Nitrogen Fracturing

ABSTRACT

Liquid nitrogen (LN_2) fracturing is a relatively new technology which can induce complex fracture networks in the much-warmer rocks under reservoir conditions. Numerous studies have investigated the fracturing mechanisms and performances of LN_2 fracturing in geothermal wells based on laboratories experiments. However, nitrogen transport in fractures does not keep liquid and cryogenic state all the time during fracturing. The phase behavior of nitrogen during fracturing is still unclear. Hence, an unsteady-state fluid flow and heat transfer 3D model for LN_2 fracturing is developed. The phase transition of nitrogen and the heat transfer between nitrogen and formation during LN_2 fracturing are taken into account. Phase distribution of nitrogen in fracture and the temperature distribution of rock around the fracture are analyzed. The results indicated that the thermal damage range around fracture is in a conical shape which is the largest around the injection point and decreased with increasing distance from the wellbore. With the increase of the flow distance in the fracture, nitrogen at the fracture tip gradually changes into supercritical state. The formation of deep fractures during LN_2 fracturing is not affected by thermal stress, but by fluid expansion and viscosity reduction. In addition, the thermal stress of rock in LN_2 fracturing is greater than that in water fracturing near the injection point. But with the increase of flow distance, the thermal stress in LN_2 fracturing is gradually lower than that in water fracturing. The main findings of this study provide a new insight into LN_2 fracturing mechanisms in high-temperature geothermal reservoirs.

1. INTRODUCTION

Geothermal energy is one of the most competitive sustainable, renewable and clean energy resources, which has the advantages of abundance, environmentally friendly and easy exploitation, etc (Shi et al., 2019). Hot dry rock (HDR), which is found at a depth of around 2-6 km with temperatures of 150-650 ℃, has enormous potential to generate electricity and is always exploited by the enhanced geothermal system (EGS). In EGS, the reservoir stimulation methods are adopted to create a number of interconnected fractures to enhance thermodynamic efficiency and heat production (Yang et al., 2019). Hydraulic fracturing is widely used, which successfully promote the commercial development of EGS reservoirs (Breede et al., 2013). Water is generally employed as the fracturing fluid in high-temperature geothermal reservoirs. Owing to the lower temperature of water, the thermal shock can be formed and create tensile stress fractures. Additionally, intensive cooling could accelerate fracture propagation and increase the fracture aperture (Cha et al., 2018; Yang et al., 2019).

However, massive hydraulic fracturing using water-based fracturing fluid poses several problems. First, the large quantities of water are required during the hydraulic fracturing process, which has pernicious effects on local water supply (Wen et al., 2020). Second, hydraulic fracturing in deep reservoir using conventional approach could trigger injection-induced earthquakes (Zang et al., 2019). Finally, because thermal equilibrium between the injected water and formation can rapidly be reached when water flows in the fractures, the thermal shock induced by the temperature differences only plays an assisting role in water fracturing, whereas pressure dominates the fracture initiation (Yang et al., 2019).

Different from hydraulic fracturing, liquid nitrogen (LN_2) fracturing is a relatively new technology for geothermal reservoir stimulation, which can provide sharper thermal shock to break the high temperature rocks and create complex fracture networks(Cha et al., 2018; Wen et al., 2020; Wu et al., 2019; Yang et al., 2019; Zhang et al., 2018).

LN_2, colorless and odorless, is an inert and clean fluid. Its boiling point at atmospheric pressure is 77 K (−196°C). The phase diagram of nitrogen is shown in **Figure 1**. There are three phase states when LN_2 is injected into the formation: liquid, supercritical and gaseous state. The temperature of LN_2 rises with the increase of migration distance in the fracture. Due to the formation pressure is generally greater than 3.4 MPa, most LN_2 changes into supercritical state (Wen et al., 2020).

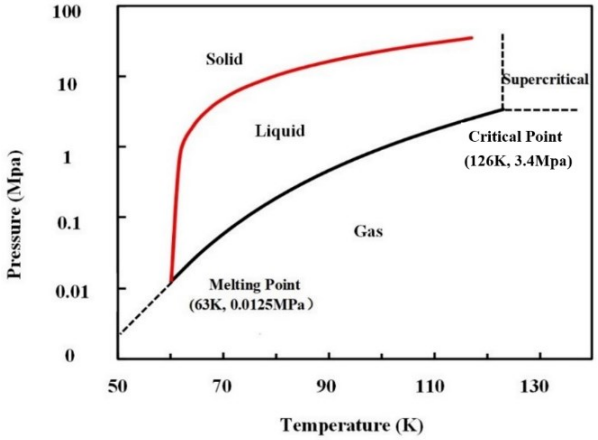

Figure 1: The phase diagram of nitrogen

Previous laboratory experiment showed that numerous thermal cracks can be formed when the high temperature rock was treated by LN_2. And the degree of thermal damage increased with the rise temperature difference between the injected LN_2 fluid and rocks (Yang et al., 2019). Moreover, the newly induced fractures can be extended farther by high-pressure fluid generated from phase-transition of LN_2 due to the high liquid/gas expansion ratio (1:694 at room temperature (20℃) and atmospheric pressure)(Cha et al., 2018; Wen et al., 2020). Hence, a complex fracture network can be formed to increase the stimulation area, which is a key for commercial heat production from EGS (Cha et al., 2017; Yang et al., 2019).

Numerous studies have investigated the fracturing mechanisms and performances of LN_2 fracturing in geothermal wells based on laboratories experiments. However, nitrogen flow in fractures does not keep liquid and cryogenic state all the time during fracturing. The transport behavior of nitrogen during fracturing is still unclear. What is the phase state of nitrogen at the crack tip? Is liquid, gaseous, or supercritical nitrogen playing a major role in fractures propagation? How widely of the reservoir can be affected by thermal stress when LN_2 migrates in fractures? These questions are crucial to the evaluate of LN_2 fracturing efficiency in field-scale, but none of them are clear.

In this paper, an unsteady-state fluid flow and heat transfer 3D model for LN_2 fracturing is developed. The phase transition of nitrogen and the heat transfer between nitrogen and formation during LN_2 fracturing are taken into account. Phase distribution of nitrogen in fracture and the temperature distribution of rock around the fracture are analyzed. Besides, the variation of thermal damage range with migration distance and injection time is obtained. Also, the thermal damage capacity of LN_2 and water in fracturing are compared. The key findings can provide a new insight into LN_2 fracturing mechanisms in high-temperature geothermal reservoirs.

2. MODEL DESCRIPTION

2.1 Model assumptions

This paper focus on giving a clear insight about the phase distribution of nitrogen and the heat transfer between nitrogen and formation during LN_2 fracturing. Therefore, the change of fluid properties, rock temperature and thermal stress are mainly studied. Since LN_2 can induce numerous thermal cracks, the nitrogen-leak-off cannot be determined. Hence, the fluid leak-off is ignored in the proposed model. This paper made the following assumptions: (1) The porosity of the rock is zero and the fracture doesn't leak off; (2) The geometry of fracture is a cube; (3) The rock is completely fixed and does not deform; (4) The fracture aperture remains constant during fracturing. (5) The extension pressure of fracture remains constant.

2.2 Mathematical model

The mass conservation equation in facture is

$$d_f \frac{\partial(\rho_f \varphi_f)}{\partial t} + \nabla_T \cdot (d_f \rho_f u_f) = 0 \tag{1}$$

Where d_f (m) is the fracture aperture, ρ_f (kg/m^3) is the fluid density, φ_f is the fracture porosity, t (s) is the time, ∇_T is the gradient operator restricted to the fracture's tangential plane, u_f is the Darcy velocity in fracture, which can be expressed by Darcy's law.

$$u_f = -\frac{k_f}{\mu_f} \nabla_T p \tag{2}$$

Where k_f (m^2) is the fracture permeability. P (Pa) is the fracture pressure.

The energy conservation equation of rock and fracture are formulated as

$$\rho_s c_{p,s} \frac{\partial T}{\partial t} - \nabla \cdot (\lambda_s \nabla T) = -Q_{f,E} \tag{3}$$

$$d_f \rho_f c_{p,f} \frac{\partial T}{\partial t} + d_f \rho_f c_{p,f} \nabla_T \cdot (u_f \cdot T) - \nabla_T \cdot (d_f \lambda_f \nabla T) = d_f Q_{f,E} \tag{4}$$

Where ρ_s (kg/m^3) is the rock density, $c_{p,s}$ (J/(kg • K)) is the heat capacity of the rock, T (K) is the temperature, λ_s (W/(m • K)) is the thermal conductivity of the rock, $Q_{f,E}$ is the heat transfer between the rock and fracture, $c_{p,f}$ (J/(kg • K)) is the heat capacity of the fluid, λ_f (W/(m • K)) is the thermal conductivity of the fluid.

The thermal stress of the rock is formulated as (Song et al., 2018)

$$F = 3K_d \alpha_T \Delta T \tag{5}$$

$$K_d = \frac{E}{3(1-2\nu)} \tag{6}$$

$$\Delta T = T - T_0 \tag{7}$$

Where F (Pa) is the thermal stress of the rock, α_T (K^{-1}) is the coefficient of thermal expansion, T_0 (K) is the initial temperature of the reservoir. E (Pa) and ν represent elastic modulus and Poisson's ratio of the rock, respectively.

2.3 Physical model

The length, width and height of the model are 200 m, 0.4 m and 30 m, respectively. And the entire computing domain is divided into 35,700 grids. The geometry is showed in **Figure 2**. The velocity inlet and pressure outlet are used as boundary conditions in the simulation. The extension pressure of fracture is 30MPa.

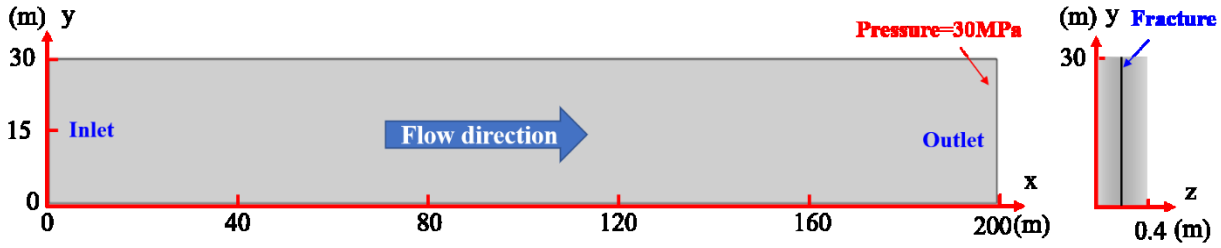

Figure 2: The geometry of model

2.4 Model validation

Before further investigation, it is necessary to verify the accuracy of the proposed model. Because there are no available experimental data obtained from LN_2 fracturing field tests for validating the numerical model. An analytical solution describing water flow and heat transfer processes in a 2D single fracture is employed to calculate the temperature in the fracture, which is given by the following equation (Barends, 2010).

$$T_f = T_0 + (T_{in} - T_0) erfc\left(\frac{\lambda_s x / (\rho_f c_{p,f} d_f)}{\sqrt{u_{in}(u_{\text{in}}\, t - x)\lambda_s / (\rho_s c_{p,s})}}\right) U\left(t - \frac{x}{u_{in}}\right) \tag{8}$$

Where T_f (K) is the temperature in the fracture, T_{in} (K) is the temperature of the injected water, $erfc$ is the complementary error function, u_{in} is the velocity of the injected water, U is the unit step function.

The input parameters of the verification are showed in **Table 1**. And the results of the numerical model and the analytical model are compared in **Figure 3**. **Figure 3(a)** illustrates the temperature variation with time at three different positions, while **Figure 3(b)** shows the temperature distribution along the fracture at various times. As can be seen from the figure, the difference between the numerical model and the analytical model results is below 1.12%, indicating that our model is quite reliable.

Table 1 The input parameters of the verification case

Items	Values
Rock density	2700 kg/m^3
Rock heat capacity	1000 J/(kg • K)
Rock heat conductivity	2.8 W/(m • K)
Injection velocity	0.2 m/s
Injection temperature	303 K
Fracture aperture	0.004 m
Rock matrix initial temperature	353 K

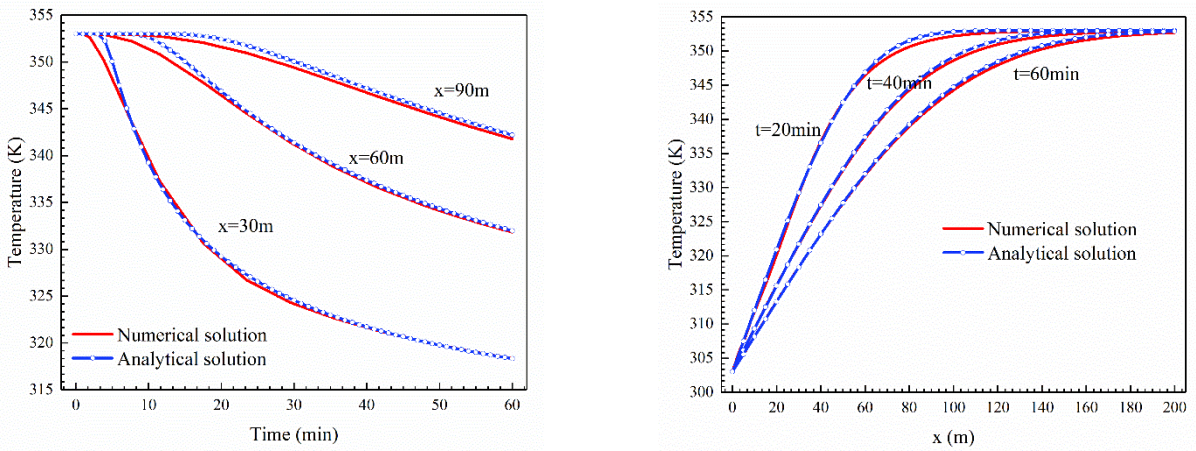

(a) Temperature variation with time at three different positions (b) Temperature distribution along the fracture at various times

Figure 3: Comparison between the numerical and analytical solutions

3. RESULTS AND DISCUSSIONS

The input parameters of case are showed in **Table 2**. In LN_2 fracturing, the injection time of LN_2 generally does not exceed 60 min, so the maximum simulation time in this study is 60 min (Grundmann et al., 1998; McDaniel et al., 1997). The temperature and density distribution of nitrogen in the fracture are simulated. Because the thermal damage is caused by thermal stress, the temperature and thermal stress distribution of rock around the fracture are simulated.

Table 2 The input parameters

Items	Values
Rock density	2700 kg/m^3
Rock heat capacity	1000 J/(kg • K)
Rock heat conductivity	2.8 W/(m • K)
Injection velocity	0.2 m/s
Injection temperature	80 K
Fracture aperture	0.004 m
Rock matrix initial temperature	573 K
Coefficient of thermal expansion	5*10^{-6} (1/K)
Rock elastic modulus	38 GPa
Rock Poisson's ratio	0.25

3.1 Temperature and thermal stress at different positions

In this section, the temperature and thermal stress at different positions (i.e. x=50 m, 10 m, 30m and 60 m) at 60 min are studied. The contour of temperature at different positions is shown in **Figure 4**. And the curves of temperature and thermal stress at different positions are shown in **Figure 5**. It is clear that the temperature difference and thermal damage range between fracture and rock near the injection point are the largest. This indicated that complex fractures are most likely to formed around the wellbore during LN_2 fracturing. With the increase of flow distance, the temperature difference between fracture and rock decreases rapidly, and the damage range of rock also decreases. It can be easily concluded that the thermal damage range around fracture is in a conical shape which is the largest around the injection point and decreased with increasing flow distance. In addition, the temperature difference between fracture and rock and the thermal stress of the rock are almost zero at 50 m. Indicating that nitrogen in the fracture has been heated to the reservoir temperature (573 K), and the maximum influence range of thermal stress in LN_2 fracturing is less than 50 m. From the temperature curve, the temperature of nitrogen is over 126 K at 5 m, indicating that nitrogen is in supercritical state here (p>3.4 MPa). So, it can be judged that nitrogen in the fracture is in supercritical state when the flow distance large than 5 m. Supercritical state is the main phase state of nitrogen in LN_2 fracturing.

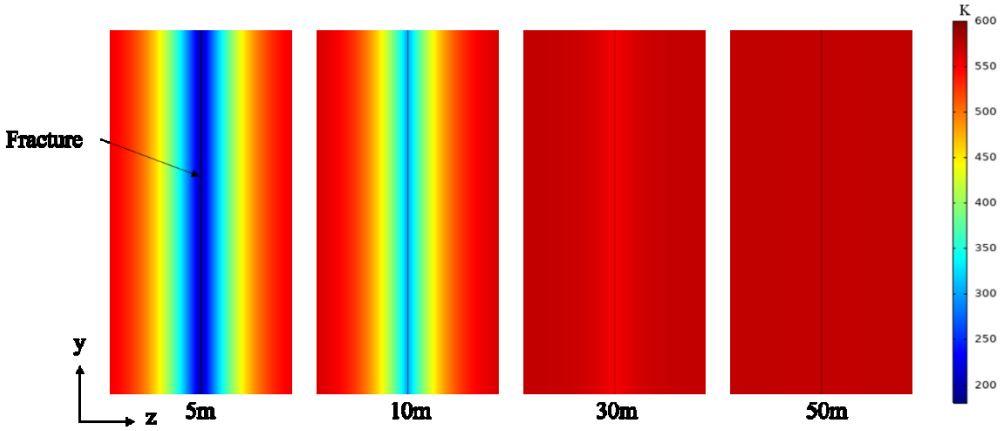

Figure 4: Temperature contours at different positions

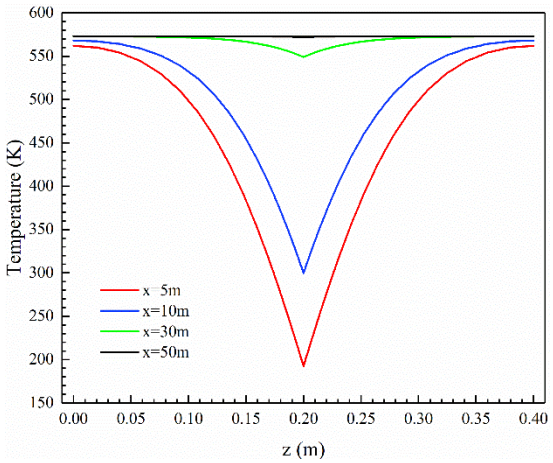

(a) Temperature variation with rock thickness at different positions

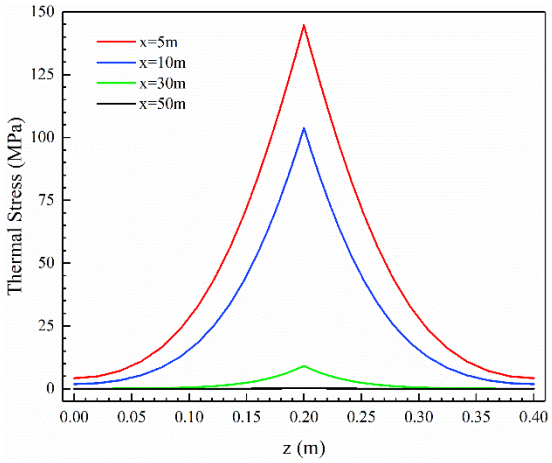

(b) Thermal stress of rock at different positions

Figure 5: Temperature and thermal stress variation with rock thickness at different positions at 60 min

3.2 Temperature and thermal stress at different times

In this section, the temperature and thermal stress distribution at various times (i.e. t=20 min, 40 min and 60 min) at 10 m are studied. **Figure 6** depicts the temperature and thermal stress at 10 m at three different times. It can be observed that the temperature of the fracture and rock decreases as the injection time increases. In addition, the thermal stress caused by the temperature difference increases gradually and diffuses to both sides of the fracture. It indicates that the injection time will affect the area of thermal damage during LN_2 fracturing. The longer the injection time is, the larger the thermal damage area will be.

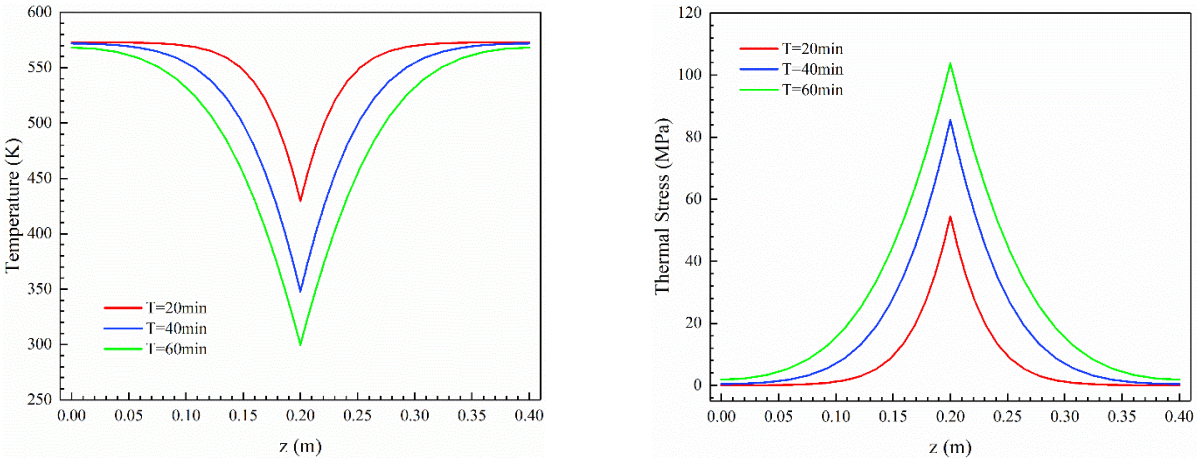

(a) Temperature variation with rock thickness at different times (b) Thermal stress variation with rock thickness at different times

Figure 6: Temperature and thermal stress variation with rock thickness at different times at 10 m

3.3 Temperature and density of nitrogen at different times

In this section, the temperature and density distribution of nitrogen along the fracture at various times (i.e. t=20 min, 40 min and 60 min) are studied. **Figure 7** shows the contour of density distribution at different times. **Figure 8** displays the temperature distribution along the fracture at various times. It can be observed that the nitrogen near the injection point is in liquid state. With the increasing flow distance, the temperature of nitrogen increases rapidly while the density decreases quickly. The temperature inside the fracture is greater than 126 K when the flow distance is greater than 2.1 m at 60 min, indicating that liquid nitrogen is transformed into supercritical nitrogen here. The critical positions at 20 min and 40 min are 1.1 m and 1.4 m respectively. It indicates that even if the wellbore insulation is very good in LN_2 fracturing, the distance of nitrogen stays liquid in the fracture is relatively short compared to the entire fracture. Supercritical nitrogen plays a major role during the LN_2 fracturing. In addition, the maximum influence distance of temperature in the fracture is 60.7 m (572.9 K) in LN_2 fracturing. Hence, thermal stress in deep fractures may not be the reason for the formation of complex fractures, but the low density and viscosity of the supercritical nitrogen and thermal expansion caused by the change of phase state are play significant roles. Ignoring the phase transition of LN_2 in fractures may lead to a misunderstanding of the fracture morphologies.

Figure 7: Density distribution along the fracture at various times

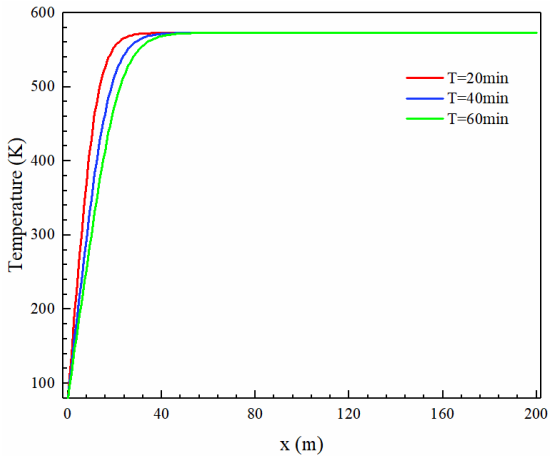

Figure 8: Temperature distribution along the fracture at various times

3.4 Comparisons of LN_2 fracturing and water fracturing

In this section, the thermal damage capacity of LN_2 and water in fracturing are compared. The injection temperature of water is 293 K, and the variation of water properties with temperature and pressure is considered in the simulation. **Figure 9** shows the contour of temperature in the LN_2 fracturing and hydraulic fracturing after 60 min. It can be seen that the temperature of nitrogen is lower than water near the injection point. With the increase of flow distance, the temperature of fracture in LN_2 fracturing increases rapidly, while the temperature in water fracturing increases relatively slowly. As a result, the temperature in water fracturing is gradually lower than that in LN_2 fracturing with the increase of flow distance. The main reason for this phenomenon is that nitrogen has a lower specific heat capacity (1.14-1.86 KJ/(kg·K)) than water (4.10-5.07 KJ/(kg·K)), so nitrogen warms up relatively quickly. **Figure 10** depicts the thermal stress distribution along the fracture wall in LN_2 fracturing and water fracturing at 60 min. Apparently, the thermal stress of rock in LN_2 fracturing is greater than that in water fracturing when the flow distance is less than 12.1 m. The thermal stress in LN_2 fracturing is the largest at the injection entrance (187.3 MPa), far greater than the tensile strength of rock (10-20 MPa). Therefore, it can be estimated that the thermal damage of LN_2 fracturing is greater than water fracturing near the injection point, and the fractures near the injection point will more complex in LN_2 fracturing. When the flow distance is greater than 12.1 m, the thermal stress of rock in LN_2 fracturing is less than that in water fracturing, indicating that the thermal damage caused by LN_2 is less than that caused by water. When the flow distance is greater than 29.5 m, the thermal stress of rock in LN_2 fracturing decreases to 10 MPa, while the distance is 93.6 m in water fracturing. Thus, it can be concluded that the maximum influence range of thermal stress in LN_2 fracturing is lower than that in water fracturing. It is further proved that the formation of deep fractures during LN_2 fracturing is not affected by thermal stress, but by fluid expansion and viscosity reduction.

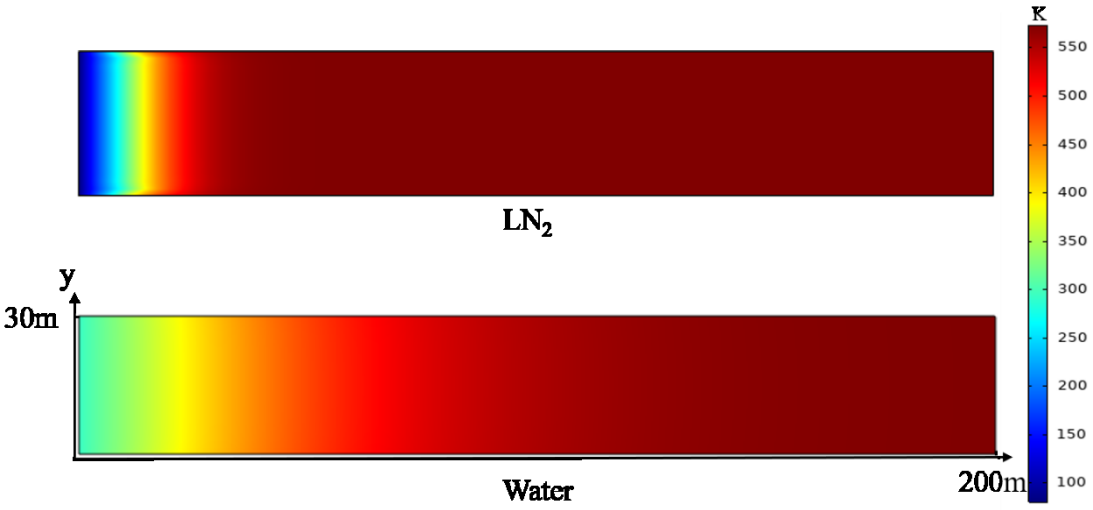

Figure 9: Temperature distribution along the fracture at 60 min

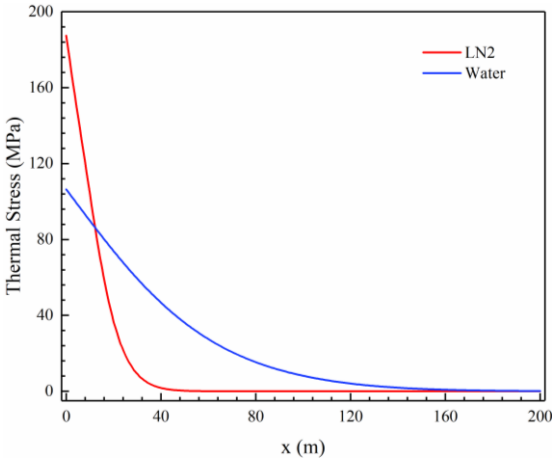

Figure 10: Thermal stress distribution along the fracture wall at 60 min

4. CONCLUSIONS

This study aims to better understand the phase distribution of nitrogen and the heat transfer between nitrogen and formation during LN_2 fracturing. An unsteady-state fluid flow and heat transfer 3D model for LN_2 fracturing is developed. The change of nitrogen properties in fracture and the temperature distribution of rock around the fracture are analyzed. Additionally, the variation of thermal stress range with migration distance and injection time is obtained. The following conclusions can be drawn in this work.

- The thermal damage range around fracture is in a conical shape which is the largest around the injection point. The damage range decreased with increasing flow distance.
- Injection time will affect the area of thermal damage during LN_2 fracturing. The longer the injection time is, the larger the thermal damage area will be.
- Supercritical nitrogen plays a major role during the LN_2 fracturing. With the increase of the migration distance in a fracture, nitrogen at the fracture tip gradually changes into supercritical state.
- The thermal stress of rock in LN_2 fracturing is greater than that in water fracturing near the injection point. But with the increase of flow distance, the thermal stress in LN_2 fracturing is gradually lower than that in water fracturing.
- The formation of deep fractures during LN_2 fracturing is not affected by thermal stress, but by the fluid expansion and viscosity reduction.

ACKNOWLEDGEMENTS

The authors would like to acknowledge Youth Program of National Natural Science Foundation of China (52004299), the International Cooperation and Communication Program (Grant No. 52020105001), National Science Fund for Distinguished Young Scholars (No.51725404).

REFERENCES

Barends, F., 2010. Complete solution for transient heat transport in porous media, following Lauwerier, SPE Annual Technical Conference and Exhibition. Society of Petroleum Engineers.

Breede, K., Dzebisashvili, K., Liu, X. and Falcone, G.: A systematic review of enhanced (or engineered) geothermal systems: past, present and future. *Geothermal Energy*, **1**(1), (2013), 4.

Cha, M., Alqahtani, N.B., Yao, B., Yin, X., Kneafsey, T.J., Wang, L., Wu, Y.-S. and Miskimins, J.L.: Cryogenic fracturing of wellbores under true triaxial-confining stresses: experimental investigation. *Spe Journal*, **23**(04), (2018), 1,271-1,289.

Cha, M., Alqahtani, N.B., Yin, X., Kneafsey, T.J., Yao, B. and Wu, Y.-S.: Laboratory system for studying cryogenic thermal rock fracturing for well stimulation. *Journal of Petroleum Science and Engineering*, **156**, (2017), 780-789.

Grundmann, S.R., Rodvelt, G.D., Dials, G.A. and Allen, R.E., 1998. Cryogenic nitrogen as a hydraulic fracturing fluid in the devonian shale, SPE Eastern Regional Meeting. Society of Petroleum Engineers.

McDaniel, B., Grundmann, S.R., Kendrick, W.D., Wilson, D.R. and Jordan, S.W., 1997. Field applications of cryogenic nitrogen as a hydraulic fracturing fluid, SPE annual technical conference and exhibition. Society of Petroleum Engineers.

Shi, Y., Song, X., Li, J., Wang, G., Zheng, R. and YuLong, F.: Numerical investigation on heat extraction performance of a multilateral-well enhanced geothermal system with a discrete fracture network. *Fuel*, **244**, (2019), 207-226.

Song, X., Shi, Y., Li, G., Yang, R., Wang, G., Zheng, R., Li, J. and Lyu, Z.: Numerical simulation of heat extraction performance in enhanced geothermal system with multilateral wells. *Applied energy*, **218**, (2018), 325-337.

Wen, H., Yang, R., Huang, Z., Zheng, Y., Wu, X. and Hu, X.: Numerical simulation of proppant transport in liquid nitrogen fracturing. *Journal of Natural Gas Science and Engineering*, **84**, (2020), 103657.

Wu, X., Huang, Z., Zhang, S., Cheng, Z., Li, R., Song, H., Wen, H. and Huang, P.: Damage analysis of high-temperature rocks subjected to LN 2 thermal shock. *Rock Mechanics and Rock Engineering*, **52**(8), (2019), 2585-2603.

Yang, R., Huang, Z., Shi, Y., Yang, Z. and Huang, P.: Laboratory investigation on cryogenic fracturing of hot dry rock under triaxial-confining stresses. *Geothermics*, **79**, (2019), 46-60.

Zang, A., Zimmermann, G., Hofmann, H., Stephansson, O., Min, K.-B. and Kim, K.Y.: How to reduce fluid-injection-induced seismicity. *Rock Mechanics and Rock Engineering*, **52**(2), (2019), 475-493.

Zhang, S., Huang, Z., Huang, P., Wu, X., Xiong, C. and Zhang, C.: Numerical and experimental analysis of hot dry rock fracturing stimulation with high-pressure abrasive liquid nitrogen jet. *Journal of Petroleum Science and Engineering*, **163**, (2018), 156-165.